Fibre-Reinforced Intumescent Fire Protection Coatings as a Fire-Safe Confining Material for Concrete Columns

Fibre-Reinforced Intumescent Fire Protection Coatings as a Confining Material for Concrete Columns

Zafiris Triantafyllidis[1] and Luke A. Bisby[2]

[1] Research Associate; The University of Edinburgh, Institute for Infrastructure and Environment, Edinburgh, United Kingdom; Email: z.triantafyllidis@ed.ac.uk *(corresponding author)*

[2] Professor, Chair of Fire and Structures; The University of Edinburgh, Institute for Infrastructure and Environment, Edinburgh, United Kingdom; Email: luke.bisby@ed.ac.uk

Abstract

This paper considers a novel, alternative application of fibre-reinforced epoxy-based intumescent coatings as potential materials for strengthening concrete columns. An experimental programme is presented examining the compressive behaviour of unreinforced concrete cylinders at ambient temperature that are confined with fibre-reinforced intumescent wraps. It is demonstrated that these advanced composite coatings can provide effective passive confinement to concrete, achieving ultimate axial strength and strain enhancements that are comparable to those of conventional FRP wraps. The enhancements are also shown to be reasonably predicted by existing confinement models for FRP-confined concrete. The results demonstrate the strong potential of these fire protection materials as alternative strengthening systems for reinforced concrete columns, potentially eliminating the need for additional passive fire protection that is common with conventional fire-rated FRP wrapping systems.

Keywords: Fibre-reinforced intumescent coatings, FRIC, fibre-reinforced polymers, concrete column strengthening, FRP wrapping, confinement, fire resistance, fire protection, insulation.

1 Introduction

1.1 Background

An important and credible concern associated with the use of externally bonded fibre-reinforced polymer (FRP) materials in structural strengthening applications is their comparatively poor mechanical performance at the elevated temperatures that would be rapidly experienced in a fire. Their tensile and bond strength decrease considerably at moderately elevated temperatures near the glass transition temperature of their polymer matrix (typically 50-120^{o}C for ambient-cured resins), whereas thermal decomposition of these polymers generally occurs at temperatures higher than 300-400^{o}C [1]. Current design guidelines for FRP-strengthened reinforced concrete (RC) structural elements suggest that the strengthening effects of an externally bonded FRP material should be neglected in fire, unless it can be shown that the FRP system remains effective during fire exposure [2, 3]. To ensure that strengthened structural elements achieve the fire resistance ratings prescribed in codes, supplemental passive fire protection (PFP) systems are often installed to the exterior of the bonded FRP systems in the form of spray-applied coatings or insulation boards [3].

However, various research studies involving standard fire (furnace) testing [4-7] showed that even if fire protection is provided, it is very difficult in practice to maintain an epoxy-based strengthening system below its glass transition temperature for the typical minimum standard fire resistance durations of 30 to 60 minutes required by building design regulations or guidelines (e.g. [8]). These findings have also been corroborated by observations in real compartment fire tests [9]. Despite this fact, experimental and numerical research [5-7, 10, 11] demonstrated that FRP-strengthened RC elements can withstand prolonged standard fire exposures (greater than four hours) when insulated with supplemental PFP systems, even if the glass transition temperature of the FRP is exceeded relatively early during fire exposure. Whilst the effectiveness of the FRP is lost early during fire exposure in such installations, the PFP coating insulates the substrate concrete and reinforcing steel and delays the degradation of their mechanical properties, thus maintaining the overall load carrying capacity at a level sufficient to carry the imposed fire limit state loads [5, 10].

The above implies that, in most situations, FRP strengthening is needed at ambient temperature (to provide the ultimate limit state design capacity) but is not necessarily essential during fire, because the existing unstrengthened (*but* fire-protected) member can typically achieve the required fire resistance rating even if the FRP is rendered ineffective. This design reality is a result of the reduced actions that are considered in the fire limit state, with load ratios being less than 0.5 in

most practical design cases [12]. On the contrary, supplemental fire protection is needed during fire (unless the existing member has been significantly overdesigned originally with respect to fire resistance) but not at ambient conditions. This holistic structural fire engineering design philosophy – i.e. considering the fire resistance of FRP-strengthened structural elements rather than the FRP strengthening systems alone – was first described by Kodur et al. [13], and is now widely recommended in design guidelines for FRP-strengthened RC structures [2, 3].

1.2 Fibre-Reinforced Epoxy Intumescent Coatings for Concrete Confinement

The requirement for additional passive fire protection to improve the fire resistance of strengthened structural elements leads, however, to substantially increased on-site disruption and installation costs, particularly since PFP systems are often proprietary (and hence expensive). The attractiveness of externally bonded FRP materials as easy and cost-effective strengthening solutions is therefore sometimes compromised, due to the increased downtimes from the follow-on installation of fire protection and the need for additional wet trades on site. This paper introduces a novel application of fibre-reinforced intumescent coatings (FRICs) as an alternative wrapping material for strengthening or retrofitting concrete columns by confinement. Such a system can strengthen a column at ambient temperature but also inherently provide it with on-demand protection in the event of a fire, thus eliminating the need for supplemental PFP that is typical for fire-safe (fire-rated) conventional FRP wrapping systems, with clear benefits as regards the cost and speed of installation of the strengthening scheme.

Intumescent coatings are reactive PFP materials that protect the (typically metallic) substrates on which they are applied by expanding upon heating into a thick, porous char layer with low thermal conductivity. Epoxy-based thick-film intumescent coatings are primarily applied where protection from severe hydrocarbon fires and durability to harsh environments is required [14], such as in oil & gas, petrochemical and other industrial applications. During installation, the wet intumescent epoxy is typically reinforced with carbon and/or glass fibre meshes to improve the performance of the comparatively weak protective char layer upon expansion in the severe design fire exposures that are considered for such environments [15], thus ensuring char integrity for prolonged fire durations.

Despite the fact that the embedded fibre mesh reinforcement is considered only as a means of retaining and stabilising the expanded insulating char in current fire protection systems, in their unreacted state (i.e. under normal service conditions) FRICs are essentially lightly reinforced FRP

materials. Previous experimental studies undertaken by the authors have shown that the tensile properties of unreacted epoxy intumescent coatings can be enhanced substantially by embedding carbon fibre reinforcement aligned in the principal loading direction [16]. Thus, except for their current function as thermal protection systems during a potential fire, FRICs with suitable mesh architecture (i.e. suitable fibre contents and orientations) could also offer the significant advantage of providing confinement to concrete columns at ambient temperature, within a single strengthening and fire protecting system. While recognizing that the confining effectiveness is likely to be lost relatively quickly in the event of a fire, due to softening of the epoxy matrix (as in the case of a conventional FRP wrap), the intumescence and charring of the reactive coating will insulate the concrete substrate and steel reinforcement. In this case, the same fibre mesh that provides the high strength and stiffness to the epoxy intumescent matrix for confining the concrete plays a dual role in retaining the expanding char of the coating when exposed to fire (as is the current practice for intumescent fire protection of steel structures subjected to hydrocarbon and jet fires). As a result of this hybrid functionality, the fire endurance of the column under the increased fire limit state loads in the strengthened case could be prolonged by delaying the degradation of the mechanical properties of concrete and steel. This is in line with the fire resistance design philosophy for FRP-strengthened RC elements described above [13], since in most cases it is neither possible (for realistic fire durations and reasonable PFP thicknesses) nor necessary to maintain the strengthening system below its glass transition temperature using external insulation; it is only necessary instead to insulate the pre-existing member sufficiently, and to ensure that the amount of strength enhancement from the externally applied strengthening system is limited to reasonable levels [2, 3].

Fibre-reinforced intumescent coatings are well established as highly effective fire protection materials (albeit typically targeted to steel structural elements and processing equipment) due to the continuous development in the past four decades driven by the fire hazard mitigation needs in the energy and processing industries. Although there is no reported scientific research on applications of intumescent coatings for fire protecting concrete (most likely due to the historically good fire performance of RC structures, which do not typically require additional PFP), FRICs are expected to perform (at least) satisfactorily in a fire for the case of protected concrete. The fire performance of the coatings is therefore not treated in this paper; the current paper's aim is to investigate the confining effectiveness of FRICs at ambient temperature, in order to provide a proof-of-concept for their use as

hybrid structural strengthening and fire protection materials for concrete columns. This paper presents the results of an experimental programme aimed at studying the axial compressive behaviour of unreinforced concrete cylinders at ambient temperature that are laterally confined with FRIC wraps incorporating different reinforcing fibre meshes. The strengthening efficiency of carbon FRIC wraps is assessed and compared with that of conventional non-intumescent CFRP wraps, and with predictions from existing confinement models that are widely used for designing FRP-wrapped concrete columns, to assess their validity for design and analysis of column strengthening schemes with the proposed novel FRIC system.

2 Experimental Programme

2.1 Test Matrix and Specimen Details

The experimental programme consisted of concentric uniaxial compression tests on two sets of plain concrete cylinders conducted at ambient temperature. The first set of tests (Series 1) involved 15 small-scale concrete cylinders with heights of 200 mm and diameters of 100 mm. Twelve of these were confined with an epoxy intumescent coating reinforced with four different candidate fibre reinforcement meshes/fabrics of differing fibre weights and stiffness to investigate their respective impacts on the effectiveness of the confinement. For each type of specimen tests were performed in triplicate to verify the repeatability of the results. These tests were exploratory as regards the potential fibre reinforcing materials that could be considered. The objectives were to determine a suitable carbon fibre weight in the circumferential direction that could exert adequate confining stresses on the concrete, to verify the ability of the comparatively thick intumescent epoxy to transfer stresses and anchor the fibres in the hoop direction, and to observe the failure modes for the FRIC systems.

For the second set of tests (Series 2), a purpose-made heavyweight carbon fibre mesh was developed, sourced, and implemented. Nine concrete cylinders with a height of 450 mm and diameter of 150 mm were tested; the cylinder dimensions in this series were chosen so that (i) the effects of frictional lateral restraint from the loading platens are minimised due to the 3:1 aspect ratio of the cylinder and (ii) the applied thickness of the wet intumescent matrix can be better controlled compared to the exploratory small cylinders of Series 1 (both points are discussed in greater detail in the following sections). Three specimens were confined with the FRIC system, three with a conventional FRP wrap (i.e. with standard non-intumescent epoxy resin), and three were left unwrapped as control specimens. Both types of wrap comprised precisely the same heavyweight

carbon fibre mesh reinforcement, to make direct comparisons between the confining capability of the new FRIC system against an FRP wrap with equivalent hoop strength and stiffness.

2.2 Confining Materials

The intumescent matrix used in the FRIC wraps is a proprietary two-part epoxy coating that is suitable for hydrocarbon fire protection in the industrial oil and gas sector. For all FRIC-wrapped specimens, a nominal 'dry film' thickness of 10 mm was chosen. Since no data are currently available on the fire performance of intumescent-coated concrete columns, it was considered reasonable for the purposes of this study to adopt a mid-range thickness value, which is representative of the current application practices of this type of intumescent coatings used for fire protection of structural steel elements in industrial applications. For the conventional FRP wrap, a commercial two-part epoxy resin was used for impregnating and bonding the carbon fibre mesh to the concrete substrate.

Four different configurations of fibre reinforcement were used in the confining wraps; these are shown during the installation stages in Figure 1 below. For the lowest fibre contents a lightweight, industry-standard, biaxial hybrid fibre mesh (denoted as Mesh 1 herein) was used in single and three-layer configurations, consisting of alternating carbon tows and glass yarns with balanced weights in each orthogonal direction. To achieve higher carbon fibre volume fractions in this exploratory work (and due to the commercial unavailability of carbon fibre meshes at the time of testing), a modified unidirectional (UD) carbon fabric was used (denoted as UD_Fabric). This was modified by removing alternate carbon tows from the original fabric such that it resembles the open architecture of a mesh, as is required for reinforcing a reactive intumescent coating. In addition, an alternative biaxial mesh consisting of PBO fibres was considered; this mesh is currently used in cementitious matrix composites for the rehabilitation of concrete and masonry structures and was included simply to trial an additional fibre and mesh type that has already been proven effective when embedded in a thick, comparatively brittle matrix [17]. The Young's modulus and density of PBO fibres are comparable to those of carbon fibres (270 GPa and 1.56 g/cm^3, respectively, for PBO [18], as compared to 240 GPa and 1.80 g/cm^3 for high strength carbon), thus it was considered that the PBO fibre mesh was indicative of the behaviour of a biaxial carbon mesh of similar fibre weight. Finally, a bespoke, heavyweight, biaxial carbon fibre mesh (denoted as Mesh 2) was developed in collaboration with the intumescent coating's manufacturer and was used for the FRIC and FRP wraps of test Series 2. It must be noted that in all of the respective meshes/fabrics described above, high strength carbon

fibres were used with moduli and ultimate tensile strains ranging between 230-240 GPa and 1.5%-1.7%, respectively, according to the manufacturers' datasheets. In the following discussions, the specimens of Series 1 are denoted with the name of their respective reinforcing mesh, whereas the specimens of Series 2 (that were both reinforced with Mesh 2) are simply denoted FRIC and FRP, respectively, to distinguish between the intumescent and conventional matrices.

The details of the wrapping materials used in the test programme and their key tensile properties determined from coupon testing are summarised in Table 1. These are expressed in terms of the tensile strength and modulus per unit width of the material, so that direct comparisons can be made between the thick FRIC and thin FRP composites. The measured failure stress and elastic modulus values obtained from coupon tests are comparatively low with respect to those of conventional FRP laminates, but it is important to note that this is an artefact of the unusually large thickness of the epoxy matrix of the specimens; this is clearly dictated by the fire protection requirements that the intumescent coatings will have to meet rather than mechanical considerations. An extensive discussion on the tensile behaviour of the composite intumescent epoxy when reinforced with these meshes/fabrics is avoided herein; specific details regarding the mechanical characterisation programme and the respective stress-strain responses can be found in [16, 19]. All coupons reinforced with the heavyweight Mesh 2 and UD fabric were characterised by a linear elastic stress-strain response; however, those reinforced with Mesh 1 displayed some degree of non-linearity (more pronounced for coupons with the single Mesh 1 layer), which is due to the low volume fraction of fibres in the material. For all coupons, failure was controlled by fibre rupture, since the elongation capacity of intumescent epoxy matrix is considerably greater than that of the respective fibres (a measured ultimate tensile strain of 2.44%).

It must be noted that no coupon tests were performed for the PBO mesh, because of the unavailability of additional mesh material at the time of testing. However, this is not considered critical, since this particular mesh was only used indicatively for the reasons described above; the wrapped cylinder results are simply included herein to show the effectiveness of this wrap in confining concrete. However, PBO fibres cannot be recommended with certainty as alternative reinforcement to carbon fibres in this case, partly because of their considerably higher cost than carbon, and due to the lack of evidence regarding their long term durability when embedded in the intumescent matrix, as opposed to the widely used carbon and glass fibres.

(a) Mesh 1 *(b) PBO Mesh* *(c) UD Fabric* *(d) Mesh 2* *(e) FRIC wrap* *(f) FRP wrap*

Figure 1: Installation of the reinforcing meshes ((a) to (d)), and finished FRIC (e) and FRP (f) wraps.

Table 1: Details of the wrapping materials used in the test programme.

Specimen/wrap type		Type of reinforcement	Fibre weight in warp (hoop) direction	No. of mesh layers	Matrix type and nominal thickness	Coupon tensile strength per unit width (kN/m)	Coupon tensile modulus per unit width (kN/m)	Coupon ultimate tensile strain (%)
Series 1	Mesh1	Biaxial carbon/glass fibre mesh	12 g/m^2 carbon; 18 g/m^2 glass	1	Intumescent, 10 mm	140	13,720	1.52
	3×Mesh1	Biaxial carbon/glass fibre mesh	12 g/m^2 carbon; 18 g/m^2 glass	3	Intumescent, 10 mm	164	13,900	1.42
	PBO_Mesh	Biaxial PBO fibre mesh	70 g/m^2	1	Intumescent, 10 mm	*	*	*
	UD_Fabric	Unidirectional carbon fabric	115 g/m^2	1	Intumescent, 10 mm	281	18,830	1.54
Series 2	FRIC (Mesh2)	Biaxial carbon fibre mesh	290 g/m^2	1	Intumescent, 10 mm	413	36,420	1.32
	FRP (Mesh2)	Biaxial carbon fibre mesh	290 g/m^2	1	Standard epoxy, 2mm	482	34,440	1.43

* Coupon test results not available for this wrap type.

2.3 Specimen Preparation

The cylinders of Series 1 were cast with concrete of intentionally low strength (23.8 MPa at the time of testing), which was mixed in the laboratory with a pan-type mixer. The cylinders of Series 2 were cast from ready-mix concrete with similar specified mix proportions and target strength class (C20/25); however, the mean cylinder strength of the delivered concrete was measured (at the time of testing) as 34.5 MPa. The age of the concrete ranged between 30 and 40 days at the time of wrapping, and three to four months at the time of testing. The specimens were cured in a conditioned laboratory environment at ambient temperature and relative humidity. Before installing the wraps, loose particles and dust were removed from the concrete surface with a stiff brush and compressed air blasting. The FRIC systems were hand-applied by trowel on the concrete surface, in multiple layers up to the target thickness of 10 mm. For specimens reinforced with a single mesh layer, this

was placed approximately at the mid-thickness of the coating, whereas for the three layers of Mesh 1, a single continuous mesh piece was wrapped spirally around the specimen with approximately 2 mm of the intumescent matrix applied in between subsequent mesh layers. The warp direction rovings of the meshes were oriented in the hoop direction, whereas the mesh overlap was 100 mm in the case of the small cylinders of Series 1 and 120 mm for the cylinders of Series 2, with approximately 1 mm of coating applied between the overlapping mesh parts in each case. An identical orientation and overlap was used in the FRP-wrapped cylinders, for which the mesh was saturated with epoxy and applied in a wet lay-up process.

2.4 Test Setup and Instrumentation

The specimens were tested monotonically under concentric uniaxial compression to failure. The cylinders of Series 1 were tested using an Instron 600LX universal testing machine at a crosshead displacement rate of 0.5 mm/min. The cylinders of Series 2 were tested using a 2000 kN capacity hydraulic cylinder installed within a self-reacting structural frame, which was driven by a manually controlled Enerpac hydraulic power pack, with the load applied at a rate of approximately 100-150 kN/min (5.7-8.5 MPa/min). Despite varying slightly between tests, the loading rate was constant during each individual test and is not expected to have influenced the results. The smaller cylinders were rotationally restrained at both ends during testing by the compression platens of the Instron 600LX machine, while the larger cylinders were rotationally restrained at the base and effectively pinned at the top by bearing against the spherical head of a compression load cell.

Axial and hoop strains were measured optically using Digital Image Correlation (DIC) and the GeoPIV code [20]. In the case of the FRIC- and FRP-wrapped specimens of Series 2, electrical resistance foil gauges were also bonded at mid-height of the cylinders, and two linear potentiometers (LP) were attached to the top loading platen to measure the total axial displacement, and thus the global axial strain of the specimen. The DIC strain measurement setup is shown in Figure 2(a). The strain measurement field was the full face of the specimen opposite the mesh overlap in the case of the small cylinders (Series 1), while in Series 2 the camera field of view covered only the central 250 mm of the cylinders' height. The bottom and top 100 mm were omitted in this case to increase the image resolution (and hence the strain measurement accuracy) over the strain measurement region of interest, since concrete dilation is affected near the column ends by frictional lateral restraint from the steel loading platens [21-23]. The locations of the virtual and physical (foil) strain gauges are

shown in Figure 2(b). Axial strains were calculated as the average of a horizontal array of pixel patch pairs with a gauge length of 100 mm, and with patch pairs spaced 2 mm apart. The width of this array was chosen as 50 mm (i.e. equal to the hoop strain gauge length). Hoop strains were measured over the full captured height of the specimens, with pixel patch pairs spaced along the centreline (2 mm apart) with a gauge length of 50 mm. The pixel patches defined for hoop strain were also used to obtain the indicative variation of axial strain along the height of the specimens (however localised since it was measured along single lines in this case) from patch pairs with a gauge length of 30 mm. To minimise light reflection and to allow pixel tracking during DIC analysis, a black and white texture was applied on the wrapped cylinders. Optical strain was measured at a frequency of 0.2 Hz, whereas all other measurements (including load and crosshead stroke) were acquired at 10 Hz.

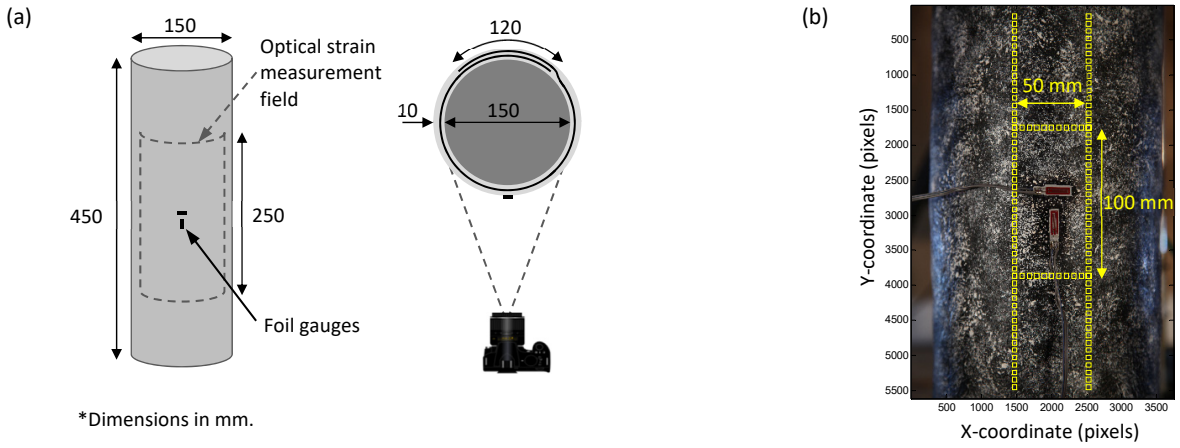

Figure 2: (a) Camera and strain gauge arrangement; and (b) pixel patch array used in DIC analysis.

3 Results and Discussion

3.1 Confined Response of the Wrapped Cylinders

Test data regarding the compressive strength, axial strains, and hoop strains of the wrapped specimens are given in Table 2, and the observed responses in terms of axial stress versus axial and hoop strains are shown in Figure 3. Significant enhancements were recorded with respect to the strength and ultimate axial strain for all confined cylinders, which overall displayed the typical compressive behaviour expected for passively confined (FRP-wrapped) concrete.

For the small-scale cylinders of Series 1, average compressive strength enhancement ratios, f_{cc}/f_{co}, ranged from 1.63 for specimens reinforced with the lightest Mesh 1, up to 2.29 for those reinforced with the modified unidirectional carbon fabric. Average ultimate axial strain of the wrapped

cylinders was up to approximately 4.5 times higher than that of unconfined concrete. The DIC-measured axial strains displayed in this case large discrepancies between specimens of the same type, even at stresses lower than the unconfined strength of concrete. Ultimate values are given in Table 2; coefficient of variation (CoV) values up to 0.40 were observed for those. Axial strains deduced from the testing machine's crosshead displacement are plotted instead of the DIC values in Figure 3(a), since they were more consistent between specimen types (CoV of ultimate values up to 0.11), representing the average total strain on the cylinders, as opposed to the more localised values measured by DIC.

All specimens reinforced with the PBO mesh, the UD carbon fabric, and Mesh 2 displayed axial stress-strain responses comprising an approximately linear secondary branch beyond the strain corresponding approximately to the unconfined concrete strength. In the case of the specimens with one or three layers of Mesh 1, this secondary branch was characterised by reduced confining stiffness at hoop strains higher than approximately 1.5%. This is due to the gradual rupture of the carbon and glass rovings and the non-linearity of the intumescent matrix that is governing the response in hoop tension, because of the very low fibre volume fraction. Figure 3(a) displays clearly that, as expected, the confined strength of the coated cylinders and the stiffness of the secondary branch of the stress-strain responses increased when the intumescent matrix was reinforced with meshes/fabrics of higher fibre weights.

The intumescent-coated cylinders of Series 2 displayed the typical approximately bilinear compressive behaviour of passively confined concrete, which was indeed very similar to their FRP-wrapped counterparts. The FRIC and the conventional FRP wraps provided equivalent strengthening effects, with the mean compressive strength enhancement being 42% and 43%, respectively. The confined ultimate axial strains were in general higher for the FRIC-wrapped cylinders compared to their FRP counterparts; ultimate strain values determined from the total axial displacement were on average 4.8 and 3.2 times higher than the unconfined concrete strain at peak stress, for the FRIC and FRP wraps respectively.

Table 2: Experimental results.

Specimen Type		Peak Stress (MPa)		f_{cc}/f_{co}	Axial Strain at Peak Stress (%)						$\varepsilon_{cu}/\varepsilon_{co}$	Ultimate Hoop Strain (%)						Hoop Strain Efficiency		
					Stroke*		DIC		Strain Gauge		(Stroke)	DIC_{ave}†		DIC_{max}		Strain Gauge		DIC_{ave}†	DIC_{max}	Strain Gauge
		Ave.	±SD		Ave.	±SD	Ave.	±SD	Ave.	±SD		Ave.	±SD	Ave.	±SD	Ave.	±SD			
Series 1	Unwrapped-1	23.4	23.8 ±0.3	0.98	0.37	0.42 ±0.08	0.50	0.56 ±0.06	–		0.87	0.20	0.27 ±0.06	0.44	0.55 ±0.09	–		–	–	–
	Unwrapped-2	24.0		1.01	0.51		0.60		–		1.21	0.28		0.58		–		–	–	–
	Unwrapped-3	24.0		1.01	0.39		0.61		–		0.92	0.31		0.62		–		–	–	–
	Mesh1-1	38.5	38.8 ±0.4	1.62	2.13	2.03 ±0.13	1.58	1.51 ±0.46	–		5.04	1.91	1.88 ±0.03	2.33	2.25 ±0.21	–		0.78	0.96	–
	Mesh1-2	38.6		1.62	1.87		1.93		–		4.43	1.88		2.40		–		0.77	0.99	–
	Mesh1-3	39.2		1.65	2.08		1.02		–		4.92	1.84		2.02		–		0.75	0.83	–
	3×Mesh1-1	46.2	46.0 ±0.3	1.94	2.34	2.16 ±0.20	2.46	1.92 ±0.58	–		5.53	1.80	1.69 ±0.15	2.20	2.00 ±0.25	–		0.74	0.90	–
	3×Mesh1-2	46.1		1.94	2.20		1.99		–		5.20	1.74		2.08		–		0.71	0.85	–
	3×Mesh1-3	45.6		1.92	1.95		1.31		–		4.61	1.53		1.72		–		0.63	0.71	–
	PBO_Mesh-1	50.1	49.8 ±1.0	2.10	1.80	1.90 ±0.14	2.00	1.53 ±0.41	–		4.27	1.14	1.29 ±0.13	1.33	1.47 ±0.12	–		‡	‡	–
	PBO_Mesh-2	48.7		2.05	1.85		1.24		–		4.38	1.32		1.54		–		‡	‡	–
	PBO_Mesh-3	50.7		2.13	2.06		1.34		–		4.87	1.40		1.54		–		‡	‡	–
	UD_Fabric-1	54.6	54.4 ±1.3	2.30	2.27	2.07 ±0.18	2.42	1.66 ±0.67	–		5.38	1.46	1.35 ±0.09	1.60	1.45 ±0.14	–		0.95	1.04	–
	UD_Fabric-2	52.9		2.22	1.98		1.17		–		4.69	1.29		1.34		–		0.84	0.87	–
	UD_Fabric-3	55.6		2.34	1.96		1.39		–		4.63	1.30		1.41		–		0.84	0.91	–
Series 2	Unwrapped-4	35.0	35.3 ±0.5	0.99	0.31	0.31 ±0.01	0.22	0.25 ±0.05	–		1.03	0.16	0.13 ±0.05	0.40	0.39 ±0.01	–		–	–	–
	Unwrapped-5§	*28.7*§		*0.81*§	*0.37*§		*0.23*§		–		–	–		–		–		–	–	–
	Unwrapped-6	35.7		1.01	0.30		0.28		–		0.97	0.09		0.38		–		–	–	–
	FRIC-1	54.0	50.1 ±3.4	1.53	1.56	1.46 ±0.09	1.77	1.44 ±0.32	1.55	1.65 ±0.13	5.10	1.18	1.19 ±0.05	1.58	1.48 ±0.11	1.79	1.42 ±0.32	0.90	1.20	1.35
	FRIC-2	48.0		1.36	1.39		1.14		1.61		4.55	1.14		1.36		1.31		0.87	1.03	0.99
	FRIC-3	48.3		1.37	1.44		1.43		1.80		4.71	1.25		1.51		1.18		0.95	1.14	0.89
	FRP-1	49.8	50.3 ±2.5	1.41	1.00	0.97 ±0.15	1.00	1.15 ±0.21	*0.61*‖	1.34 ±0.57	3.28	0.66	0.70 ±0.16	1.44	1.30 ±0.16	0.90	0.98 ±0.26	0.46	1.01	0.63
	FRP-2	53.0		1.50	1.10		1.39		1.74		3.60	0.87		1.33		1.26		0.61	0.93	0.88
	FRP-3	48.2		1.37	0.81		1.08		0.94		2.66	0.57		1.13		0.76		0.40	0.79	0.53

* Strains calculated from crosshead displacements and corrected for loading frame compliance for Series 1, and from linear potentiometer measurements for Series 2.

† Average value over central 100 mm for Series 1, over central 250 mm for Series 2.

‡ Coupon tests were not performed on PBO mesh.

§ Specimen Unwrapped-5 failed prematurely by flexure; not considered in the calculation of average results.

‖ Strain gauge partially debonded before failure; not considered in the average ultimate axial strain calculation.

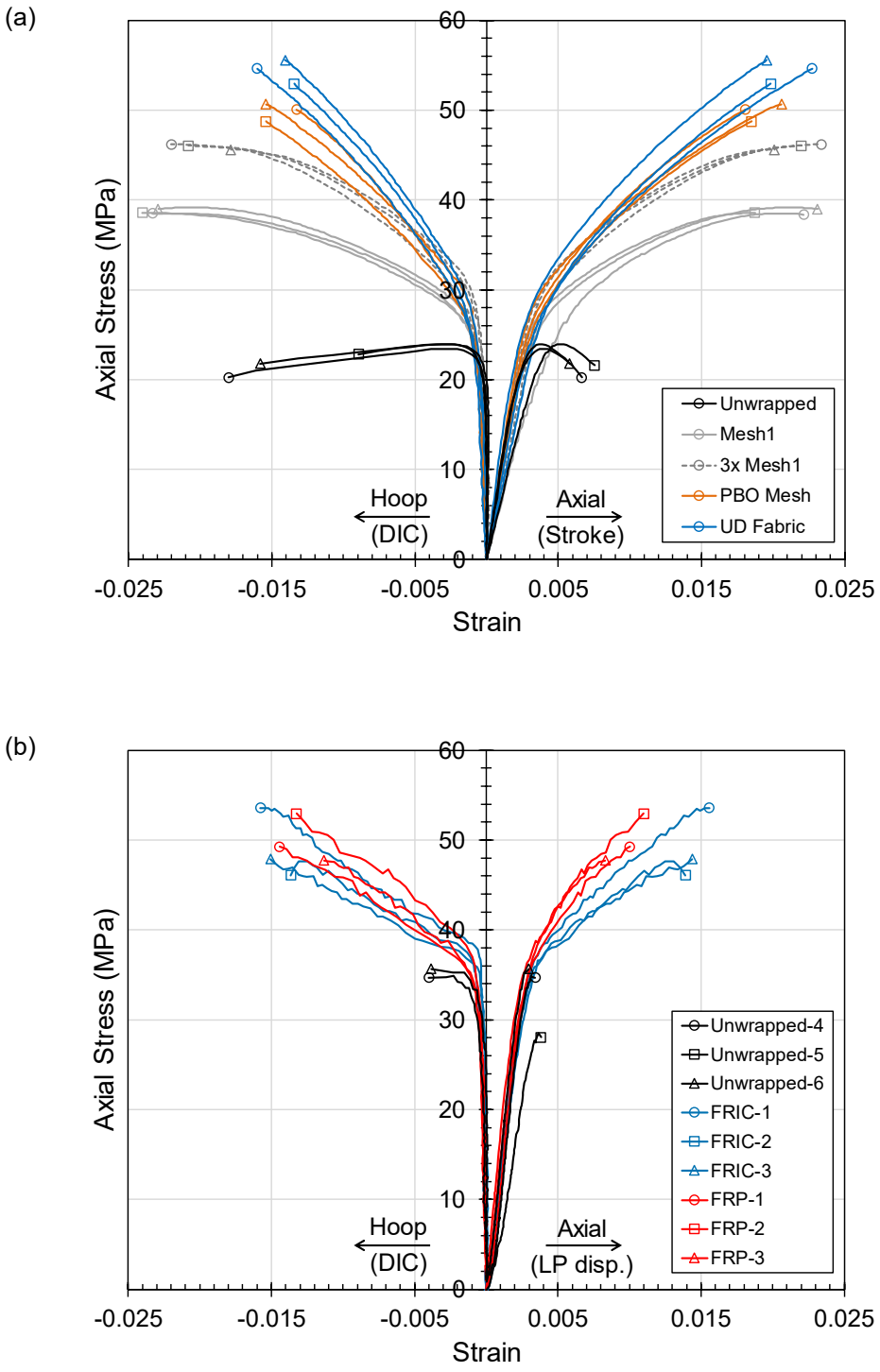

1 Figure 3: Axial stress versus axial and peak hoop strain of (a) Series 1 and (b) Series 2 specimens.

3.2 Strain Variation and Hoop Strain Efficiency

3.2.1 Series 1

All wrapped specimens failed by tensile rupture of the intumescent coating in the hoop direction, with a vertical crack initiating at the most highly strained point and propagating vertically towards the cylinder ends. Figure 4 shows a representative photograph of a specimen immediately after rupture, as well as the hoop and axial strain distributions over the specimens' height immediately before failure. Hoop and axial strains have been shown in [23] to vary considerably both over the height and around the perimeter of FRP-wrapped cylinders, and they are expected to vary similarly for the FRIC-wrapped cylinders. However, the strain distributions measured at the front face of the cylinders presented herein provide a good illustration for the hoop strains developed at the ultimate condition, despite being only local to a single radial coordinate (diametrically opposed to the overlap centre). These are characterised by large variations over the height of all cylinders, with considerably lower hoop strains recorded near the specimen ends. This indicates that substantial frictional restraint exists between the cylinder and the loading platens, which results in additional confining stresses near the cylinders' end regions [21-23]; this is discussed in greater detail in the following subsection. Despite the large variability over the cylinders' height, peak hoop strains did reach values that were close to the ultimate tensile failure strain of the respective materials, albeit only locally, in most cases close to the cylinder's mid-height.

Table 2 gives values of the hoop strain efficiency (defined as the ratio of the hoop strain at rupture over the ultimate tensile strain determined from coupon tests) calculated for the peak and average hoop strains for all cylinders; averaged efficiency values ranged between 0.63 and 0.95, while the peak efficiency values were close to unity for most specimens. Strain efficiencies are not reported for the PBO specimens because no direct tension testing was performed on coupons reinforced with this particular mesh. It is also noteworthy that the strain efficiency calculation for all specimens reinforced with Mesh 1 takes into account the tensile failure strain of the unreinforced intumescent matrix, rather than that of the fibre-reinforced coupons. Peak hoop strains measured for those specimens were considerably higher (up to 49%) than the average failure strain recorded for the respective fibre-reinforced coupons tested in direct tension, and indeed very close to the average failure strain of the unreinforced matrix. This is because of the higher than specified final coating thickness of the small cylinders of Series 1, due to the difficulty in controlling thickness uniformity in each applied layer during installation for such a small cylinder diameter. Total thicknesses were found

to vary within the range of 11-16 mm around the specimens' perimeter; this resulted in even lower fibre volume fractions in the wraps compared to the respective coupons, and thus the failure mode in hoop tension was characterised by matrix cracking after fibres had ruptured. Final thicknesses were considerably more consistent for the larger cylinders of Series 2 with tolerances of ±1 mm.

As already discussed above, the DIC-measured local axial strains calculated from the averaged virtual gauge array over the central 100 mm of the cylinders' faces displayed considerable variability between different specimens. In addition, the strain distributions of Figure 4(c) indicate that large variability also exists over the height of individual specimens. The shape and magnitude of the axial strain distributions appear to be essentially random for all confined specimens, and no clear correlations could be found between the axial strains and the respective hoop strain patterns. On the other hand, the measured hoop strains exhibit general agreement between specimens of the same type regarding both their distribution shape and the peak strain values at ultimate (Figure 4(a)).

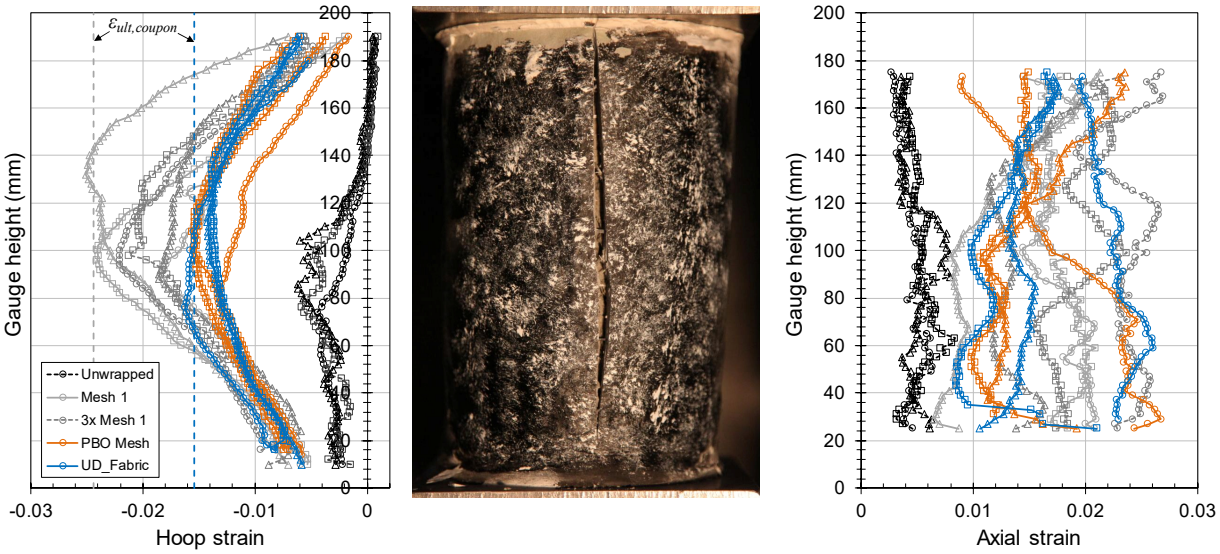

Figure 4: (a) Hoop strain variation over the cylinder height at failure, (b) typical failure mode, and (c) axial strain variation at failure, for Series 1 specimens.

Strain localisation, Boundary Restraint, and Specimen Size Effects on Measured Strength

The large variability that exists in the strain distribution of the wrapped cylinders is thought to be largely a consequence of frictional confinement at the specimen boundaries and strain localisations within the concrete [23, 24]. In uniaxial compression testing, shear stresses develop between the concrete specimen's ends and the loading platens because of the different lateral expansion of the two materials in contact, and as a result the end zones of the specimen are laterally confined by the frictional restraint at the boundary [21, 22]. Since early studies on compressive testing of concrete (e.g. [25]) it is well-appreciated that the boundary restraint and the resulting triaxially stressed zones influence the apparent compressive strength (i.e. the specimen strength, not the strength of the material) of short unconfined specimens when loaded with hardened steel rigid platens. Unless friction reducing measures are taken (e.g. by using intermediate Teflon sheets), the apparent strength increases with decreasing specimen aspect ratios, whereas these slenderness effects disappear for ratios greater than 2.0-2.5 [26]. Beyond the peak stress of unwrapped concrete specimens, localised fracture planes are known to develop within the concrete due to the confined end zones, whereas the measured deformations during the softening stage are due to the relative sliding of concrete wedges along the fracture planes [22, 27]. Strain localisation always occurs in the post-peak softening stage [22], although the way it develops as well as the slope of the descending branch of the axial stress-strain response of unconfined concrete are greatly influenced by the amount of boundary restraint, depending on the type of platens or friction-reducing measures used [21, 22]. When high friction boundary conditions exist (as in the case of conventional rigid steel platens that were used for the tests herein), cracking develops in the unconfined zones of the specimen resulting in the typical hour-glass shape failure mode, whereas the axial stress-strain response displays a relatively shallow softening branch compared to low friction boundary conditions [21, 22, 26].

Similarly to unconfined concrete, strain localisations occur in FRP-wrapped cylinders because of the formation of failure planes and the sliding of solid concrete wedges that take place in the secondary (typically) ascending branch of the confined axial stress-strain response, as shown in a numerical study by Tabbara and Karam [24]. Furthermore, Bisby and Take [23] experimentally quantified the strain variation over the surface of the FRP-wrapped cylinders using DIC, and corroborated the idea that the hoop strain variation is largely due to this strain localisation

mechanism. In [23], the authors found that the variation of hoop strains can be as high as 50% of the failure strain obtained from coupon testing, even far away from the frictionally restrained column ends, but in most cases the coupon failure strain is achieved somewhere locally on an FRP-wrapped cylinder's surface.

The variations observed for the FRIC-wrapped cylinders of Series 1 in Figure 4 are in good agreement with the findings of [23]. The high lateral restraint that is apparent from the hoop strain distribution near the ends of the small cylinders suggests that their measured compressive strength could have been affected by frictional confinement, resulting in improved load capacities for these specimens as compared to longer wrapped cylinders. The large thickness of the FRIC wraps in this case resulted in approximately 60% larger (on average) cross-sectional area of the coated cylinders compared to the unwrapped cylinders, reducing the height-to-total-diameter ratio to approximately 1.6:1 from the original 2:1 of the plain cylinder. The higher restraint from the larger area in contact with the steel platens could have partly constrained the localisation of shear failure planes, extending the influenced zones by frictional confinement, similarly to plain concrete specimens of aspect ratios lower than 2:1 as noted above. In the numerical study presented in [24], a comparison between FRP-wrapped cylinders with aspect ratios of 1:1 and 2:1 showed that shear failure planes are constrained by the proximity of the column ends in the former case, resulting in higher load capacities. The failure planes that develop from the ends towards the cylinder's centre meet before reaching it, leaving an intact core that requires further energy to mobilise the initiation of new fracture planes until ultimate failure [24]. Thus, the apparent confined strength and the stiffness of the secondary branch in the axial stress-strain response are in this case greater than for specimens of higher aspect ratios.

The effect of boundary restraint in relation to the specimen geometry is possibly one of the factors corrupting the obtained confined strength values for the FRIC-wrapped cylinders, and this may result in substantial overestimation of the strength enhancement ratios f_{cc}/f_{co}. Another important factor for this is the contribution of the thick coating in carrying a proportion of the applied axial load at higher axial strains, particularly due to the larger applied thickness than specified as discussed above. In practice the coating is under a triaxial stress state during loading instead of being stressed only in the hoop direction as idealised for conventional FRP wraps [28]. However it is not possible (and also not strictly necessary for the purposes of this particular test series) to estimate the extent of each factor's influence on the confined strength overestimation, due to (i) the high uncertainty regarding the

compressive behaviour and cross-sectional characteristics of the coating in each cylinder, and (ii) the very complex, non-uniform stress state related to frictional restraint that exists within the concrete core.

Despite the fact that the measured strength enhancement ratios of Series 1 are influenced by the structural behaviour of the specimen under the specific test conditions and are (very likely) not representative of the true confined strength of the material under uniaxial compression with the respective wraps, the obtained results from these exploratory test series showed clearly that the novel FRIC systems can indeed provide effective passive confinement to a concrete core. The composite intumescent coatings were effective in resisting high lateral expansion due to strain localisation (whatever the concrete failure mode may have been beneath the wrap), they failed by tensile rupture of the wrap reaching hoop strains very close to the measured coupon failure strain without any premature fibre pull-outs or overlap failures, and they significantly enhanced the axial deformation capacity of the wrapped concrete.

Finally, it is should be noted that the effects of boundary restraint and specimen size were realised after examining the obtained stress-strain responses and results from Series 1. The selection of the standard cylinder dimensional proportions for this exploratory series was based on the experimental practice reported in the literature, since the majority of FRP-confined concrete characterisation tests have been performed on standard cylinders of 150 mm in diameter and 300 mm in height. The smaller size adopted herein was simply due to load capacity and test space considerations regarding the specific universal testing machine that was used. Several experimental studies are available in the literature on standard concrete cylinders confined with thick fibre-reinforced cementitious composites of similar geometric proportions with the FRIC-wrapped cylinders of Series 1 (considering the target intumescent thickness of 10 mm). These cementitious wraps generally comprise of multiple layers of mesh reinforcement (usually up to 4) embedded between 3-4 mm thick layers of cement mortar. References to specific experimental studies are avoided but an extensive list can be found in a dedicated section on concrete confinement with cementitious composites in a review paper by Koutas et al. [29]. In general, the effects of specimen size (cross-section enlargement) and boundary restraint do not seem to be reported (or recognised) in the literature, although these are likely to influence the specimen behaviour to some extent, since they

are relevant to any type of concrete cylinder up to a 2:1 aspect ratio that is loaded with steel platens and no friction reducing measures (e.g. Teflon sheets) [26], as discussed above.

For the tests of Series 2 presented in the following section, the effects of boundary restraint and specimen size were rendered insignificant due to the larger aspect ratio that was adopted (3:1), and therefore the confined behaviour at the central part of the cylinder was not affected by frictional confinement. Moreover, the larger cylinder diameter of 150 mm and better thickness control during application (10±1 mm) ensured that the axial load bearing contribution of the wrap is negligible (based on a simple conservative analysis assuming linear elastic behaviour of the intumescent matrix).

3.2.2 Series 2

Figure 5 shows the hoop and axial strain distributions over the central 250 mm of the cylinders immediately prior to failure. For all cylinders failure was localised within approximately two thirds of their height; this is also evident in the observed axial and hoop strain variation, where strains appear to decrease towards one end of the specimen. This is due to an implication that arose during concrete casting, when the bottom quarter to one third of the cylinder moulds was filled with concrete of lower slump (i.e. water content) and hence slightly higher compressive strength than the rest of the specimen, thus strain localisations were more prominent at the top part. The restricted dilation of the stronger concrete zone is clearly visible in the hoop strain variation of the confined specimens within the bottom (for FRIC) or top (for FRP) 150 mm of the cylinders. The trend in the hoop strain variation of the FRP confined specimens is opposite to that of the FRIC and unconfined specimens because they had been positioned in the test frame upside-down due to strain gauge orientation and wiring arrangement issues.

The indicative axial strain distributions shown in Figure 5 appear to vary randomly over the specimen height, with no obvious correlations with the respective hoop strain profiles, except for the lower strains developed near the zones of higher strength concrete. However, there is a clear difference between the more uniform pattern in the evolution of axial strain for the FRIC specimens and the frequent/successive peaks and troughs that are apparent for the FRP specimens. This is due to localised concrete crushing for the latter, which occurred between hoop rovings of the carbon fibre mesh because of its open construction. Axial foil gauge measurements are in a good agreement with strains obtained from DIC locally, however, it is clear from the large variability over the height that these values cannot be considered as representative of the overall specimen behaviour. Axial stress-

strain responses (Figure 3) and ultimate axial strain enhancement ratios, $\varepsilon_{cu}/\varepsilon_{co}$, (Table 2) were instead determined from the total axial strains calculated from displacement measurements as discussed in Section 2.4. The measured values of the total ultimate axial strain of the FRIC-strengthened specimens were on average 51% higher than for the FRP-wrapped specimens (average strain and standard deviation were 1.46% ± 0.09% and 0.97% ± 0.15%, respectively). The respective local DIC axial strains measured from the arithmetic mean of 26 virtual gauges over a length of 100 mm at mid-height (Figure 2(b)) were 1.44% ± 0.32% and 1.15% ± 0.21%.

The hoop strain distributions of Figure 5 are characterised by large variability over the height of all cylinders. For the FRP-wrapped cylinders in the current study, peak strains developed within the bottom half of the column and low hoop strains were recorded in the higher strength zone near their top ends. Indeed, at this location hoop strains appeared to be mildly compressive at failure (although very close to zero) for two of the FRP-wrapped cylinders; this is probably because of the localised failure developing at the bottom part of the cylinder, which could have caused flexural stresses in the undamaged top part. However, the wraps did reach local hoop strains that were very close to those determined from straight coupon tests of the same material. The measured peak values of the hoop strain efficiency were between 0.79 and 1.01 for the three specimens. The average hoop strain efficiency over the total (measured) height for all three specimens was 0.47 with a standard deviation of 0.32, which is in very good agreement with the reported mean hoop strain efficiency of 0.50 ± 0.30 for CFRP-wrapped cylinders suggested in a previous study [30]. This mean strain efficiency in [30] was obtained from the statistical evaluation of a large population of hoop strains (1667 readings) from confined cylinders with aspect ratios ranging between 2:1 and 6:1, measured with the same DIC technique as used herein.

On the other hand, the FRICs developed relatively more uniform and consistent hoop strains in the central region of the cylinder, despite the fact that the zone of higher strength concrete near the base influenced their distributions. Peak hoop strains occurred near mid-height, with hoop strain efficiencies exceeding unity and ranging between 1.03 and 1.20 for the three specimens. Although local strain efficiencies that are higher than 1.0 have been observed in FRP-wrapped cylinders [23, 30], these usually arise from the statistical variation in the tensile properties of the test coupons. In the case of the FRIC-strengthened specimens, the coating sustained considerably greater hoop strains

than those observed for the tensile coupons over a larger area; the average strain efficiency over the total measured height for all three specimens was 0.90 ± 0.22.

The reason for the significantly larger failure strains reached by the FRICs in the wrapped cylinder tests than those observed in tensile coupon tests is not clear. Potential overestimation of the actual strains due to lateral movements of the specimen towards the camera is not considered as a credible source of error, since the localised foil gauge readings at mid-height are in good agreement with local DIC strains, also yielding unexpectedly high efficiency values at the point of measurement (up to 1.35). A possible explanation may be that strains measured on the surface of the coating at fibre rupture were higher than those at the fibre level due to flexing of the thick coating. This could have been a result of potential non-uniformities in the lateral dilation of the concrete core, considering the significantly higher stiffness (both axial and flexural) of the thick wrap over a quarter of the cylinders' perimeter, due to the mesh overlap. Furthermore, it is likely that at high axial strains the thick coating may be flexing to resist larger internal displacements of the sliding concrete wedges, therefore explaining the beneficial difference of 51% that was observed in the average total axial strain at ultimate condition for FRIC cylinders compared to their FRP counterparts. The FRP wraps on the other hand are prone to localised failure at discontinuities on the concrete surface caused by cracking and wedge sliding deformations, due to their lower flexural and shear stiffness than the thick intumescent coating. This effect is even more pronounced for the particular mesh-reinforced FRP wraps, and it is evidenced by the localised peaks and general variation of hoop strain in the distributions of Figure 5. However, these assumptions cannot be corroborated further with the experimental data obtained from the current study.

Figure 6 shows representative photographs of the confined cylinders after failure. All confined specimens failed by fibre rupture in hoop tension; no overlap failures or fibre pull-outs were observed. This indicates that the 120 mm overlap provided adequate bond for the carbon fibre mesh used in this application. Rupture occurred in most specimens close to the beginning of the hoop overlapping region, possibly due to the presence of geometric discontinuities at the fibre level [31]. Although failure was relatively sudden and brittle in all cases, it was less violent in the case of the FRIC-strengthened specimens. For those, fracture initiated at the most highly stressed fibre rovings and progressed vertically in the form of a straight crack, towards the top and bottom of the cylinder (Figure 6(a)), with the slit coating containing the fractured concrete core due to its higher flexural stiffness. On

the other hand, the FRP wrap split more explosively, as soon as the most highly stressed rovings reached their failure strain. It is noteworthy that in specimen FRIC-3, although cracking of the coating initiated at peak stress over a small length at the beginning of the overlap, ultimate failure occurred eventually with a vertical crack at the front face of the specimen (opposite to the overlap, see Figure 6(a)), following a slight drop in the applied axial load (refer to Figure 3(a)). In all cases, the failure initiation locations over the height of the specimen coincided with the regions of highest hoop strains in the distributions shown in Figure 5.

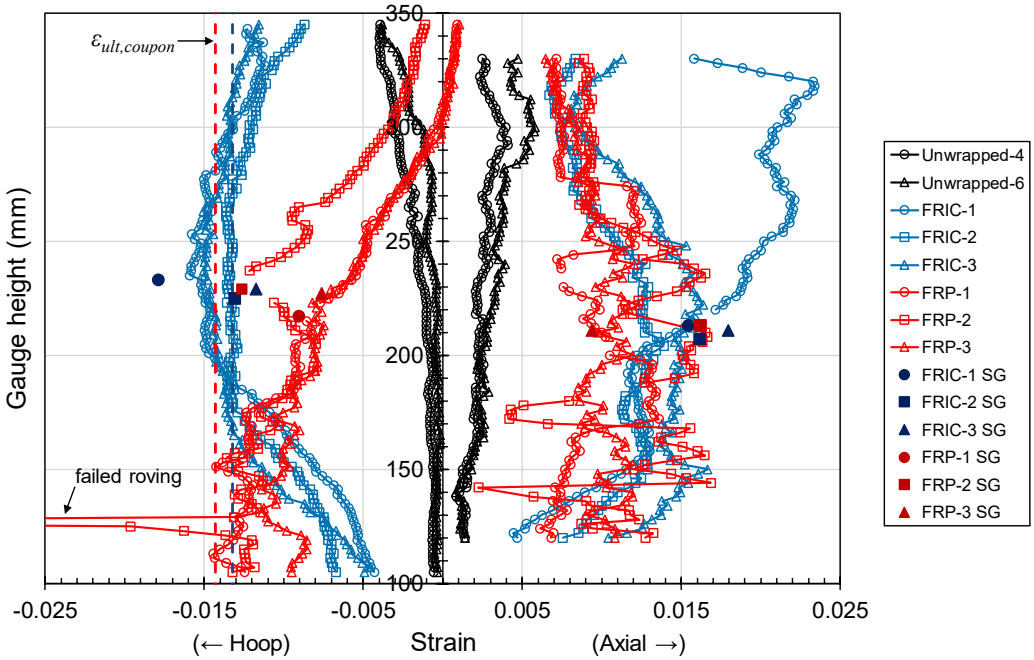

Figure 5: Axial and hoop strain variation over the specimen height at failure for Series 2 cylinders.

(a) FRIC (a) FRP

Figure 6: Representative failure modes of the confined cylinders of Series 2 (wraps shown with black and white speckle pattern applied for DIC strain measurements).

4 Prediction of the Confined Compressive Behaviour

The capability of existing FRP confinement models in predicting peak strength and ultimate axial strain for FRIC-wrapped circular cross-section columns is examined in this section, in order to assess their applicability/suitability for use in designing column strengthening schemes with the FRIC wraps. A large number of analytical and empirical models have been proposed in the literature and many extensive reviews of model performance are available with comparisons on their predictive abilities, e.g. [32-34]. For the purposes of this paper, only a selection of representative design-oriented FRP confinement models is considered for comparison with the experimental data from the FRIC- and FRP-wrapped cylinders of Series 2. Their accuracy and precision in predicting the confining performance of the FRIC wraps is evaluated in terms of the mean error (ME) and the mean absolute error (MAE), respectively, given by:

$$ME = \frac{\sum_{i=1}^{N} \frac{P_{theor} - P_{exp}}{P_{exp}}}{N} \quad (1) \qquad , \qquad MAE = \frac{\sum_{i=1}^{N} \frac{\left|P_{theor} - P_{exp}\right|}{P_{exp}}}{N} \quad (2)$$

where P is the property under consideration (f_{cc} or ε_{cu}), and N is the number of tests. However, this assessment is only indicative due to the statistically very small sample sets, and is only performed as a preliminary evaluation of the applicability of current design-oriented confinement models for column wrapping schemes using the novel intumescent system proposed herein.

4.1 Confined Strength

In the assessment of peak strength predictions, the models considered were those proposed by Lam and Teng [35], Teng et al. [36], and Rousakis et al. [37]. The expressions of these models are not included herein for brevity, although some of their merits (and thereby the reasons for their selection) are discussed below.

The well-known design-oriented stress-strain model by Lam and Teng [35] has been adopted in the design guidelines published by ACI Committee 440 [2]. A refinement to this model was proposed by Teng et al. [36] with new, more accurate expressions for the prediction of compressive strength and ultimate axial strain to be used with the existing stress-strain model of Lam and Teng [35]. These refined expressions were adopted with minor modifications in the current edition of design guidelines for cylindrical FRP-confined columns published by the Concrete Society [3]. A major weakness of Lam and Teng's expressions [35] (and indeed of most empirical confinement models) is the large uncertainty regarding the ultimate condition (i.e. hoop strain) of the FRP wraps at rupture, which on the basis of most of the available research appears to occur at strains considerably lower than the failure strain of FRP coupons in direct tension. Lam and Teng [35] considered the average hoop strain at rupture for the calculation of the confinement pressure and suggested an average hoop strain efficiency of 0.586 for CFRP-confined cylindrical columns, based on their assembled experimental data. However, the ultimate hoop strain readings reported in the literature and used for model calibration are typically measured by discrete foil gauges, the precise number and location of which is in many cases not reported [36].

Teng et al. [36] addressed the uncertainty in ultimate hoop strain that characterises the large database used by Lam and Teng [35] by correlating their refined expressions based only on test data obtained by their research group under standardised test conditions, to improve the accuracy of their model. Hoop strain measurements at rupture were taken in this case as the average value from five strain gauges outside the overlapping zone at the specimen's mid-height, ignoring the considerably lower strains that are measured on the overlap. According to the observations of Lam and Teng [38], the lower strains at the overlap are only a result of the larger thickness of the wrap but do not result in a lower confining pressure at this location. Hence, Teng et al. [36] suggested that the reduced average hoop strain by taking these readings into account is unrepresentative of both the strain capacity of the wrap and the dilation properties of concrete. As discussed previously, however, hoop strain varies considerably both around the circumference as well as the height of FRP-wrapped

columns, thus it is extremely difficult to capture the true ultimate condition of the wrap using discrete bonded foil gauges. At rupture of the wrap, hoop strains very close to the coupon failure strain are achieved in most cases, even though only locally, as shown by [23] and [30], and confirmed by the experimental hoop strain distributions of the FRIC- and FRP-wrapped cylinders in the previous sections. Therefore, it is questionable whether the average hoop strain (measured either by foil gauges or over the total specimen surface in the case of DIC) yields an accurate confinement pressure at ultimate, since peak hoop strain values are in most cases very close to the actual tensile failure strain of the FRP material.

The model proposed by Rousakis et al. [37] was selected for assessment because it has an advantage over other empirical models in that it accounts for the ultimate hoop strain indirectly, and requires knowledge of only the tensile rigidity of the FRP wrap and the unconfined strength of concrete. According to Rousakis et al. [37], the peak strength enhancement, f_{cc}/f_{co}, can be empirically related to the modulus of elasticity and the nominal thickness of the dry fibre fabric, which are properties that can be more confidently defined (and commonly found in manufacturer's datasheets), thus reducing the error in the predicted peak strength enhancement. Indeed, in a relatively recent review [34] with one of the largest assembled databases of experimental results, the proposed expression by Rousakis et al. [37] is found to yield the lowest mean absolute error (MAE) amongst the available FRP confined strength models applicable to cylindrical columns (10.5%).

Figure 7(a) compares the performance of the models considered for predicting the confined strength of wrapped cylinders of Series 2. In all cases, the calculated MAE with respect to the experimental results is lower than typical error values reported for model predictions previously compared with large databases (e.g. [32-34]). The most conservative predictions are those by Lam and Teng [35] under predicting peak strength by 4.5% on average for both the FRIC- and the FRP-wrapped columns. Similarly, the design equation of the Concrete Society [3] yields more conservative results than the original expression that it adopts [36], because Concrete Society suggests a hoop strain efficiency of 0.6 at rupture, along with a slightly modified constant in the peak strength equation. The models of Teng et al. [36] and Rousakis et al. [37] exhibited very similar precision and accuracy (MAE of 4.7%-5.0% for the FRIC-wrapped specimens and 3.3% for the FRP-wrapped specimens; ME very close to zero in both cases).

It is noteworthy that the failure strain used in the model of Teng et al. [36] was the coupon failure strain, $\varepsilon_{ult,coupon}$, rather than the average ultimate hoop strain that was considered in the model's calibration. The error in the predictions of this particular model, using the peak hoop strain, $\varepsilon_{h,rup}$, measured from DIC, is also included in Figure 7(a) for comparison. The strength in this case was over predicted by 2.7% on average for the FRIC-wrapped specimens, due to the fact that the apparent hoop strains at rupture were considerably higher than the coupon failure strains, as discussed previously (peak hoop strain efficiencies up to 1.20 and average values up to 0.95 – refer to Table 2). On the contrary, the strength in the case of FRP-wrapped cylinders was under predicted by 4.2% using peak hoop strain, i.e. with somewhat higher mean error than predictions using the uniaxial failure strain (ME=-1.6%).

Although the errors in either case could be considered very low compared to the typical mean errors reported in the literature using large statistical data sets, they suggest that the use of the coupon failure strain is more rational than the measured hoop strain (either peak or average over the column height). The higher hoop strains that were measured on the thick FRIC wraps are possibly unrepresentative of the strain at the level of the carbon fibres (which governs failure), possibly due to flexural effects on the thick epoxy, as discussed in Section 3.2.2. Furthermore, the FRP wraps may have achieved local hoop strain efficiencies even closer to 1.0 than those measured by DIC (Table 2), since rupture initiated outside the strain measurement field in most cases.

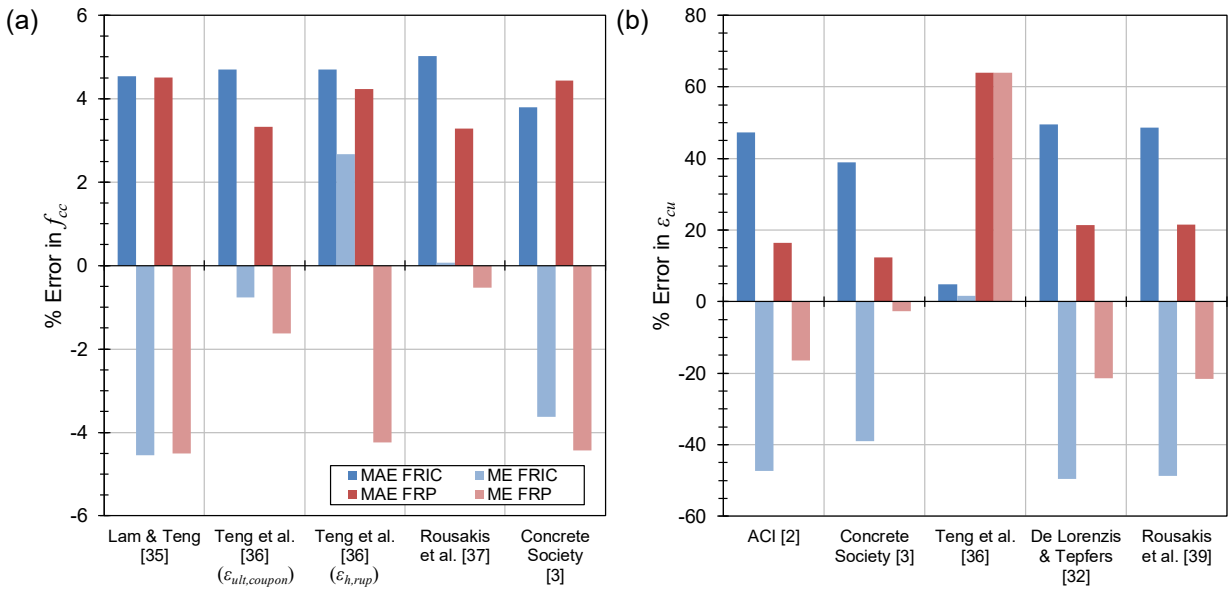

Figure 7: Mean error in (a) confined strength and (b) ultimate axial strain predictions, as compared with the test data from Series 2.

4.2 Ultimate Axial Strain

The examined ultimate axial strain models were the expression proposed in ACI Committee 440 [2], the expression proposed by Teng et al. [36] both in its original form using the coupon failure strain and including a hoop strain efficiency of 0.6 as recommended by the Concrete Society [3], and finally the model by Rousakis et al. [39]. The latter is based on the strain model by De Lorenzis and Tepfers [32] (also included for comparison), and both of these have the benefit of bypassing the effects of hoop strain efficiency by lumping it in the parameters determined via regression analysis. These two models display the lowest MAE between those examined in published comprehensive model reviews [32-34].

The errors in the predicted ultimate axial strains (based on total strain values from LP measurements) are summarised in Figure 7(b). These were considerably higher than the errors in predicted peak strength, this being generally the case also in the available literature when the accuracy of predictive expressions for strain is compared to those for strength [32-34]. All models under predicted the ultimate strain of the specimens, except for that of Teng et al. [36] in the case of the FRP-wrapped cylinders; this was characterised by a mean error of 63%. At the same time, this model yielded the lowest error for the FRIC-wrapped cylinders with a MAE of 4.8% and ME of 1.6%. All the other models consistently under predicted the ultimate strain, with mean errors being between 39%-50% for the FRIC-wrapped cylinders and between 12%-22% for the FRP-wrapped cylinders.

The much larger error in the prediction of axial strain than for strength is, according to [32], due to the greater sensitivity of strain equations to the value of ultimate confining pressure, compared to those for strength prediction. In their review of the available strain models, De Lorenzis and Tepfers [32] observed that all equations over predicted ultimate strain, but the use of a reduced effective hoop strain reduced the prediction error greatly. This is reasonable since all models assume uniform strain over the height of the column [33], hence they overlook the large strain variation (both axial and hoop) that is now known to exist over the height and around the perimeter of the column. This is illustrated by the differences shown in Figure 7(b), where the Teng et al. model [36] yields very unconservative predictions for the FRP-wrapped cylinders, in contrast to the Concrete Society's model [3] (i.e. the same equation considering a hoop strain efficiency of 0.6). These strain variations play an important role in the observed axial strain of the cylinders, as shown in Figure 5. FRIC wraps reached more uniform hoop strain efficiencies close to (and exceeding) 1.0 over a significantly larger proportion of the specimen's height compared to the FRP wraps, and consequently achieved greater ultimate axial

strains. Current axial strain models that assume uniform (peak or average) hoop strain distributions cannot capture such differences.

Furthermore, the recorded strain values are considerably influenced by the strain measurement method used, the location of measurement and gauge length, because of the axial strain variation over the surface of a test specimen. The ultimate strain data reported in the literature and used for model calibration are characterised by high scatter largely because of the different testing conditions and measurement methods employed by various researchers. Teng et al. [36] recognised the need for consistency in the data used for their model development, using only standardised measurements obtained by their own research group. However, there seems to be no consensus currently amongst researchers regarding the test and strain measurement conditions that would yield 'reliable' data, primarily due to the lack of understanding of the strain localisation mechanisms that cause the high variations measured on the specimens' surface. There is nonetheless a need to rationalise the test methods and strain measurements required for the reliable calibration of empirical design-oriented models taking into account the effects of strain localisation caused by shear friction in confined concrete. Research on understanding and evaluating those is available in the literature [23, 24, 27, 40], however, there is a need for further investigations in this field to enhance understanding.

5 Conclusions

The tests presented in this paper have clearly demonstrated that fibre-reinforced epoxy intumescent coatings can provide effective lateral confinement to concrete cylinders at ambient temperature, when wraps are applied with fibres of suitable weight oriented in the circumferential (hoop) direction. The following conclusions can be drawn from this study:

- The novel FRIC wrapping system proposed herein was effective in resisting lateral dilation and exerting confining stresses to the concrete core up until tensile rupture of the fibres, and resulted in considerable enhancements of the axial load bearing capacity and deformability of the specimens. The confining performance of the FRIC wraps reinforced with the biaxial carbon fibre mesh developed for this study was very similar to counterpart FRP wraps consisting of the same reinforcing mesh and conventional non-intumescent epoxy resin. The average peak strength and ultimate axial strain increased by 42% and 480%, respectively, for the FRIC-wrapped specimens, with only minor differences between the FRIC and FRP wraps.

- The small-scale cylinder geometry that was considered in Series 1 (100 mm in diameter, 2:1 aspect ratio) may not be suitable for measuring the confined strength of short FRIC-wrapped concrete columns (or perhaps confined with thick composite wraps, in general). The measured strength appears to be influenced by the increased frictional confinement near the specimen ends, due to the large coating thickness, and the fact that the coating may carry a significant proportion of the applied axial load at higher axial strains – due to its comparatively large compressive cross-sectional area for this specific cylinder size. On the other hand, for the larger cylinders of Series 2 (150 mm diameter, 3:1 aspect ratio) the coating thickness did not appear to affect the confined strength.
- The available existing design-oriented FRP confinement models that were examined herein were found to reasonably predict the peak strength and ultimate axial strain of the FRIC-confined specimens. Model predictions for the FRIC-wrapped cylinders were characterised in all cases by similar errors compared to those for FRP-wrapped cylinders. This suggests that empirical models developed for the latter could possibly be applied in designing strengthening schemes with the novel FRIC systems developed herein, subject to further testing to increase the statistical dataset and potential refinement of the empirically determined parameters.

The results demonstrate that FRICs clearly have a strong potential as alternative strengthening systems for reinforced concrete columns, since they can provide confinement to resist increased loads at ambient temperature. At the same time, FRICs can thermally protect the substrate concrete and the steel reinforcement in the event of a fire, by intumescing and charring, thus potentially eliminating the need for additional passive fire protection that is common with conventional fire-rated FRP wrapping systems. However, additional research is required to study the fire protection performance of the proposed novel FRIC systems when applied to concrete substrates, and to optimise the required coating thicknesses for this application to make use of the proposed hybrid functionality with confidence.

Finally, further investigations are necessary for understanding the effects of strain localisation caused by the formation of shear failure planes in FRP-wrapped (and similarly FRIC-wrapped) concrete. The evaluation of the experimental results and the predictive performance of representative existing design models highlighted the need for confinement models that rationally account for the large strain variation (both axial and hoop) that is known to exist over the surface of wrapped

columns. Although research has been published on this issue by other researchers, it appears that there is no consensus in the research community regarding the test conditions and measurement methods that would yield reliable data for model development and calibration, addressing the strain variability at the ultimate condition of the wraps.

Acknowledgments

The authors would like to acknowledge the support of the UK Engineering and Physical Sciences Research Council (EPSRC) and the School of Engineering of the University of Edinburgh.

Notation

List of symbols used in this paper:

f_{cc}	Compressive strength of confined concrete
f_{co}	Compressive strength of unconfined concrete
ε_{co}	Axial strain at peak stress of unconfined concrete
ε_{cu}	Ultimate axial strain of confined concrete
$\varepsilon_{h,rup}$	Hoop strain at rupture of FRP wrap
$\varepsilon_{ult,coupon}$	Tensile failure strain of coupon

References

[1] J.P. Firmo, J.R. Correia, L.A. Bisby, Fire behaviour of FRP-strengthened reinforced concrete structural elements: A state-of-the-art review, Composites Part B: Engineering 80 (2015) 198-216. DOI: http://dx.doi.org/10.1016/j.compositesb.2015.05.045.

[2] ACI Committee 440, ACI 440.2R-17 Guide for the Design and Construction of Externally Bonded FRP Systems for Strengthening Concrete Structures, American Concrete Institute, Farmington Hills, MI, USA, 2017.

[3] The Concrete Society, Technical Report No. 55: Design guidance for strengthening concrete structures using fibre composite materials, Camberley, United Kingdom, 2012.

[4] H. Blontrock, L. Taerwe, P. Vandevelde, Fire Testing of Concrete Slabs Strengthened with Fibre Composite Laminates, FRPRCS-5: Proceedings of the fifth international conference on fibre-reinforced plastics for reinforced concrete structures, 16-18 July 2001 Cambridge, UK. 2001, pp. 547-556.

[5] L.A. Bisby, V.K.R. Kodur, M.F. Green, Fire Endurance of Fiber-Reinforced Polymer-Confined Concrete Columns, ACI Structural Journal 102(6) (2005) 883-891. DOI: 10.14359/14797.

[6] B. Williams, L. Bisby, V. Kodur, M. Green, E. Chowdhury, Fire insulation schemes for FRP-strengthened concrete slabs, Composites Part A: Applied Science and Manufacturing 37(8) (2006) 1151-1160. DOI: http://dx.doi.org/10.1016/j.compositesa.2005.05.028.

[7] D. Cree, E.U. Chowdhury, M.F. Green, L.A. Bisby, N. Bénichou, Performance in fire of FRP-strengthened and insulated reinforced concrete columns, Fire Safety Journal 54 (2012) 86-95. DOI: http://dx.doi.org/10.1016/j.firesaf.2012.08.006.

[8] HM Government, Approved Document B: Fire Safety (Volumes 1 and 2), The Building Regulations 2010, NBS (part of RIBA Enterprises Ltd), Newcastle Upon Tyne, United Kingdom, 2011.

[9] T.J. Stratford, M. Gillie, J.F. Chen, A.S. Usmani, Bonded Fibre Reinforced Polymer Strengthening in a Real Fire, Advances in Structural Engineering 12(6) (2009) 867-878. DOI: 10.1260/136943309790327743.

[10] L.A. Bisby, M.F. Green, V.K.R. Kodur, Modeling the Behavior of Fiber Reinforced Polymer-Confined Concrete Columns Exposed to Fire, Journal of Composites for Construction 9(1) (2005) 15-24. DOI: 10.1061/(asce)1090-0268(2005)9:1(15).

[11] B. Williams, V. Kodur, M.F. Green, L. Bisby, Fire Endurance of Fiber-Reinforced Polymer Strengthened Concrete T-Beams, ACI Structural Journal 105(1) (2008) 60-67. DOI: 10.14359/19069.

[12] A.H. Buchanan, A.K. Abu, Structural Design for Fire Safety, 2nd ed., John Wiley & Sons Ltd, Chichester, UK, 2017.

[13] V.K.R. Kodur, L.A. Bisby, M.F. Green, FRP Retrofitted Concrete Under Fire Conditions, Concrete International 28(12) (2006). DOI:

[14] T.A. Roberts, L.C. Shirvill, K. Waterton, I. Buckland, Fire resistance of passive fire protection coatings after long-term weathering, Process Safety and Environmental Protection 88(1) (2010) 1-19. DOI: http://dx.doi.org/10.1016/j.psep.2009.09.003.

[15] G.P.J. Boyd, G.K. Castle, Reinforcement System for Mastic Intumescent Fire Protection Coatings Comprising a Hybrid Mesh Fabric, US patent application 5,433,991, 1995.

[16] Z. Triantafyllidis, L. Bisby, Fibre-Reinforced Epoxy Intumescent Coatings for Strengthening and Fire Protecting Steel Beams, 7th International Conference on FRP Composites in Civil Engineering - CICE 2014, 20-22 August 2014 Vancouver, Canada. 2014.

[17] A. Nanni, A New Tool for Concrete and Masonry Repair: Strengthening with fiber-reinforced cementitious matrix composites, Concrete International 34(4) (2012). DOI:

[18] Toyobo, PBO Fiber Zylon® - Technical Information (Revised 2005.6), Toyobo Co., Ltd., Osaka, Japan, 2005.

[19] Z. Triantafyllidis, Structural Enhancements with Fibre-Reinforced Epoxy Intumescent Coatings, PhD Thesis, The University of Edinburgh, Edinburgh, Scotland, United Kingdom, 2017.

[20] D.J. White, W.A. Take, M.D. Bolton, Soil deformation measurement using particle image velocimetry (PIV) and photogrammetry, Géotechnique 53(7) (2003) 619-631. DOI: https://doi.org/10.1680/geot.2003.53.7.619.

[21] M.D. Kotsovos, Effect of testing techniques on the post-ultimate behaviour of concrete in compression, Matériaux et Construction 16(1) (1983) 3-12. DOI: 10.1007/bf02474861.

[22] M.R.A. van Vliet, J.G.M. van Mier, Experimental investigation of concrete fracture under uniaxial compression, Mechanics of Cohesive-frictional Materials 1(1) (1996) 115-127. DOI: https://doi.org/10.1002/(SICI)1099-1484(199601)1:1<115::AID-CFM6>3.0.CO;2-U.

[23] L.A. Bisby, W.A. Take, Strain localisations in FRP-confined concrete: new insights, Proceedings of the ICE - Structures and Buildings 162(5) (2009) 301-309. DOI: https://doi.org/10.1680/stbu.2009.162.5.301.

[24] M. Tabbara, G. Karam, Numerical Investigation of Failure Localization and Stress Concentrations in FRP Wrapped Concrete Cylinders, Proceedings of the Advanced Composite Materials in Bridges and Structures, Winnipeg, Manitoba, Canada, 22-24 September, 2008; Winnipeg, Manitoba, Canada.

[25] K. Newman, L. Lachance, The Testing of Brittle Materials under Uniform Uniaxial Compressive Tests, Proceedings of the American Society for Testing and Materials 64 (1964) 1044 - 1067. DOI:

[26] J.G.M. van Mier, S.P. Shah, M. Arnaud, J.P. Balayssac, A. Bascoul, S. Choi, D. Dasenbrock, G. Ferrara, C. French, M.E. Gobbi, B.L. Karihaloo, G. König, M.D. Kotsovos, J. Labuz, D. Lange-Kornbak, G. Markeset, M.N. Pavlovic, G. Simsch, K.-C. Thienel, A. Turatsinze, M. Ulmer, H.J.G.M. van Geel, M.R.A. van Vliet, D. Zissopoulos, Strain-softening of concrete in uniaxial compression, Materials and Structures 30(4) (1997) 195-209. DOI: 10.1007/bf02486177.

[27] P. Visintin, Y. Chen, D.J. Oehlers, Size Dependent Axial and Lateral Stress Strain Relationships for Actively Confined Concrete, Advances in Structural Engineering 18(1) (2015) 1-20. DOI: 10.1260/1369-4332.18.1.1.

[28] J.F. Chen, S.Q. Li, L.A. Bisby, Factors Affecting the Ultimate Condition of FRP-Wrapped Concrete Columns, Journal of Composites for Construction 17(1) (2013) 67-78. DOI: 10.1061/(ASCE)CC.1943-5614.0000314.

[29] L.N. Koutas, Z. Tetta, D.A. Bournas, T.C. Triantafillou, Strengthening of Concrete Structures with Textile Reinforced Mortars: State-of-the-Art Review, Journal of Composites for Construction 23(1) (2019) 03118001. DOI: doi:10.1061/(ASCE)CC.1943-5614.0000882.

[30] L.A. Bisby, T.J. Stratford, The Ultimate Condition of FRP Confined Concrete Columns: New Experimental Observations and Insights, Advances in FRP Composites in Civil Engineering: Proceedings of the 5th International Conference on FRP Composites in Civil Engineering (CICE 2010), Sep 27–29, 2010 Beijing, China. 2010, pp. 599-602.

[31] J. Chen, J. Ai, T. Stratford, Effect of Geometric Discontinuities on Strains in FRP-Wrapped Columns, Journal of Composites for Construction 14(2) (2010) 136-145. DOI: 10.1061/(asce)cc.1943-5614.0000053.

[32] L. De Lorenzis, R. Tepfers, Comparative Study of Models on Confinement of Concrete Cylinders with Fiber-Reinforced Polymer Composites, Journal of Composites for Construction 7(3) (2003) 219-237. DOI: 10.1061/(asce)1090-0268(2003)7:3(219).

[33] L.A. Bisby, A.J.S. Dent, M.F. Green, Comparison of Confinement Models for Fiber-Reinforced Polymer-Wrapped Concrete, ACI Structural Journal 102(1) (2005) 62-72. DOI: 10.14359/13531.

[34] N. Nisticò, F. Pallini, T. Rousakis, Y.-F. Wu, A. Karabinis, Peak strength and ultimate strain prediction for FRP confined square and circular concrete sections, Composites Part B: Engineering 67 (2014) 543-554. DOI: http://dx.doi.org/10.1016/j.compositesb.2014.07.026.

[35] L. Lam, J.G. Teng, Design-oriented stress–strain model for FRP-confined concrete, Construction and Building Materials 17(6–7) (2003) 471-489. DOI: http://dx.doi.org/10.1016/S0950-0618(03)00045-X.

[36] J. Teng, T. Jiang, L. Lam, Y. Luo, Refinement of a Design-Oriented Stress–Strain Model for FRP-Confined Concrete, Journal of Composites for Construction 13(4) (2009) 269-278. DOI: 10.1061/(asce)cc.1943-5614.0000012.

[37] T. Rousakis, T. Rakitzis, A. Karabinis, Design-Oriented Strength Model for FRP-Confined Concrete Members, Journal of Composites for Construction 16(6) (2012) 615-625. DOI: 10.1061/(asce)cc.1943-5614.0000295.

[38] L. Lam, J.G. Teng, Ultimate Condition of Fiber Reinforced Polymer-Confined Concrete, Journal of Composites for Construction 8(6) (2004) 539-548. DOI: 10.1061/(asce)1090-0268(2004)8:6(539).

[39] T. Rousakis, T. Rakitzis, A. Karabinis, Empirical modelling of failure strains of uniformly FRP confined concrete columns, Proceedings of the 6th International Conference on FRP Composites in Civil Engineering – CICE 2012, 13-15 June 2012 Rome, Italy. 2012.

[40] M. Haskett, D.J. Oehlers, M.S. Mohamed Ali, S.K. Sharma, Evaluating the shear-friction resistance across sliding planes in concrete, Engineering Structures 33(4) (2011) 1357-1364. DOI: https://doi.org/10.1016/j.engstruct.2011.01.013.